# OBJECTIVE IDENTIFICATION OF CELL CYCLE PHASES AND SUBPHASES BY AUTOMATED IMAGE ANALYSIS

C. NICOLINI, F. KENDALL, AND W. GIARETTI, *Division of Biophysics, Department of Biophysics and Physiology, Temple University Health Science Center, Philadelphia, Pennsylvania 19128, U.S.A.*

ABSTRACT Frequency distributions of integrated optical density, perimeter, projection, area, form factor, average optical density, and mean dispersion path of nuclear images of Feulgen-stained HeLa S3 cells were obtained by automated image analysis at the base threshold of 0.04 OD. The mean values and standard deviations of these geometric parameters were then computed versus increasing values of threshold (0.08–0.32 OD). There is clear evidence of differential chromatin dispersion and convolution during the cycle of synchronized HeLa S3 cells at different times after selective mitotic detachment. The combination of average OD, form factor, and mean dispersion path at base threshold with the threshold dependence of nuclear morphometric parameters permits objective identification of cell cycle phases and their subphases, by characterizing variations in chromatin geometry within and between phases, regardless of whether DNA content remains constant (early G1, middle G1, late G1), varies only slightly (late G1–early S or late S–G2 transitions), or varies significantly (early S–middle S).

## INTRODUCTION

Functional and structural (1) changes of chromatin of mammalian cells during the cell cycle have been frequently reported (2, 3). Chromatin differences during the phases M, G1, S, and G2 of synchronized mammalian cells have been analyzed with respect to binding sites for ethidium bromide (1), circular dichroism spectra (1), the amount of actinomycin D bound per unit DNA (4), the sensitivity of chromatin to digestion by DNase (5), protein phosphorylation (6, 7), and other autoradiographic, physical, and chemical properties (3).

All these studies on isolated chromatin are compatible with a well-defined chromatin conformation for every phase of the cell cycle. There is of course no way to estimate the degree to which measurement artifacts are introduced during the chromatin isolation process. In this respect abundant evidence exists in the literature that the structural and functional properties of native chromatin are modified by physical alterations introduced during chromatin preparation (8, 9).

Several alternative texture analysis approaches, which allow chromatin characterization *in situ*, have been successfully applied to the study of cells (10–13) and to the

characterization of the cell cycle (14, 15). The technique of automated image analysis with the Quantimet 720 D (Cambridge Instrument Co., Inc., Monsey, N.Y.) (15–17) has been used in the present work to study: (*a*) the frequency distribution of directly measured (area, projection, perimeter, and integrated OD [IOD]) and derived (form factor, average OD, mean dispersion path [MDP]) parameters of Feulgen-stained nuclei from synchronized HeLa S3 cells at 1, 3, 5, 8, 12, 15, and 18 h after mitoses; (*b*) the dependence of mean values of these geometric parameters upon the optical density threshold in the range 0.04–0.32 OD. The results permit objective characterization of the cell cycle phases and subphases, not previously possible by other means.

## METHODS

### *Cell Culture*

Logarithmically growing HeLa S3 cells were maintained in suspension by Joklik-modified Eagle's minimum essential spinner medium (18) supplemented with 3.5% each of calf serum and fetal calf serum. Synchronization of cells was carried out in a warm room at 37°C by selective mitotic detachment (19–21). Approximately 90% of the detached cells were observed by phase contrast microscopy to be in mitoses immediately after harvesting. The detached cells were maintained in culture at 37°C for 18 h. During this period, smears were prepared in triplicate from the same culture at 1, 3, 5, 8, 12, 15, and 18 h after selective detachment (15). The triplicate smears for each post-detachment time were hydrolized with 1 N HCl for 15 min. They were stained with Schiff reagent for 50 min according to the methods of De Cosse and Aiello (22). 100 cells or more, randomly and independently selected from various regions of each slide, were studied for each post-detachment time.

### *Data Processing*

The image analyzer Quantimet 72OD was used for these studies (16). It was equipped with a plumbicon television scanner and 720D densitometer module. The scanned area was divided into 880 × 588 picture points (17). The area of each picture point was $(0.09 \times 0.09)\mu m^2$, under the condition of the present investigation: condenser aperture 1.35, 100× oil immersion planar achromat objective with open iris and a numerical aperture of 1.25, 10× internal magnification. This value was below the limit of resolution of the microscope employed (Reichert Zetopan research microscope with 100 W tungsten halogen light equipped with a 546 nm filter giving 40 nm bandwidth; C. Reidert, American Optical Corp., Buffalo, N.Y.), thus precluding significant distributional errors (17). Shading due to the optical system of lenses itself, the nonuniform illumination in the imaging device, and the nonuniform response of the plumbicon faceplate are compensated by a shading corrector. OD was calibrated as follows: 100% transmission (0.0 OD) was defined by a large clear area of the slide and 0% transmission (infinite OD) by blanking all light to the scanner. A 1.0 OD neutral density filter was then inserted into the light path (by using the same clear area of the slide) and the densitometer was adjusted by the calibration controls until a threshold setting 1.0 on the densitometer resulted. This procedure produced an overall linear calibration from 0.0 to 2.0 OD (a region where the light transfer characteristic of the plumbicon is linear [0.99]). The threshold calibration was linear throughout the operating range of the plumbicon tube. The image analyzer Quantimet is based on measuring geometric parameters of objects (i.e. Feulgen-stained nuclei) removed from the background by a simple threshold, which is linearly proportional to OD, since we use a plumbicon. Optical density thresholds were programmed as follows: the nuclear border was defined by 0.04 OD. Thus, there are 50 intervals of OD from 0.0 to 2.0 OD. The densitometer was then pro-

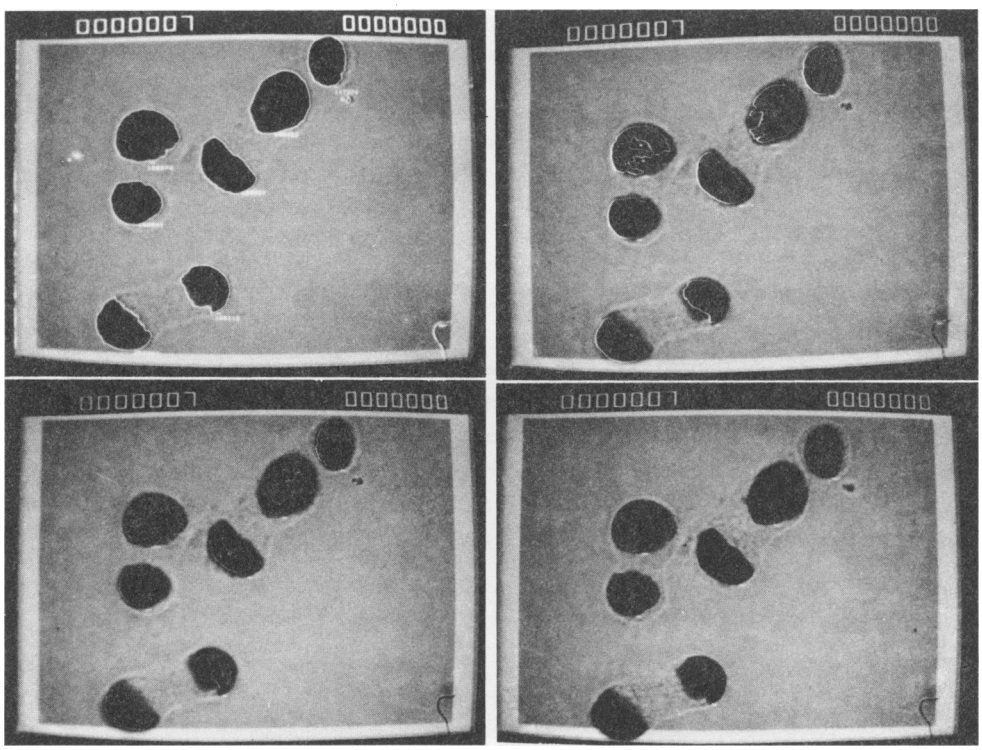

FIGURE 1 Video display of Feulgen-stained HeLa cell images projected from the microscope onto the face plate of a television scanner. The white contour lines of each cell indicate the perimeter of regions of nuclei with picture points having absorbance greater than the given absorbance threshold: 0.04 (upper left), 0.12 (upper right), 0.24 (lower left), and 0.40 (lower right).

grammed in equal optical density steps of 0.04 to obtain eight thresholds of 0.04, 0.08, 0.12, 0.16, 0.20, 0.24, 0.28, and 0.32 OD. Final system performance was checked by measuring the IOD (i.e., the sum of the densities from all picture points in the detected area) and the area of a single nucleus at seven differnt locations within the scanning field. The coefficients of variation of these parameters represent estimates of the effects of both nonuniformities and random electrical noise during the time required to make the individual measurements (about 5 min). The coefficient of variation was 2.4% for IOD and 1.0% for area. Multivariate Student $t$ two-tailed tests (23) were used for a direct comparison of the mean values of the parameters corresponding to the same threshold level for two adjacent post-detachment times (15). The significance level required to reject the null hypothesis was set in advance at 1%. For many comparisons the differences were so large (no overlap) that no test of significance was needed.

Three computer programs (24) were written to permit screening and extraction of raw values for specific parameters and subsequent statistical testing of the means and variances that resulted. We measured the following parameters for each nucleus image at the base threshold (OD = 0.04): IOD, area, projection, and perimeter. These geometric parameters were also computed at seven other OD thresholds, specifically 0.08, 0.12, 0.16, 0.20, 0.24, 0.28, and 0.32 OD (see Fig. 1). The following derived parameters were also computed from measured values: average optical density (obtained only at the base threshold, by dividing the IOD by the area), form factor (obtained by dividing the area by the square of its perimeter), and mean dispersion

path (MPD) ($A_1/Pr_i$, obtained at every threshold by dividing the area of a nuclear image at base threshold, $A_1$, by its horizontal projection at each threshold $i$, $Pr_i$). In this case the horizontal projection consisted of the linear sum of all lagging edges projected against a vertical line. MDP is related to the average distance between picture points with IOD larger than the given threshold: its value as a function of threshold may allow a quantative assessment of chromatin dispersion, based only on geometric criteria.

## RESULTS

### *Direct and Derived Parameters, at Base Threhold*

The frequency distributions of IOD (Fig. 2) of HeLa S3 cells, at various time intervals after mitosis, indicate that the cells progress through the entire cell cycle during the 18-hr period. This, combined with [$^3$H]thymidine pulse autoradiography (1) (Table I) allows assignment of the various cell populations to early G1 (1 h), middle G1 (3 h), late G1 (5 h), early S (8 h), middle-late S (12 h), G2 (15 h), and the beginning of the G1 in the new cell cycle (18 h). The corresponding frequency distributions of nuclear area and perimeters, measured at the base threshold (0.04 OD), are shown in Fig. 3. They

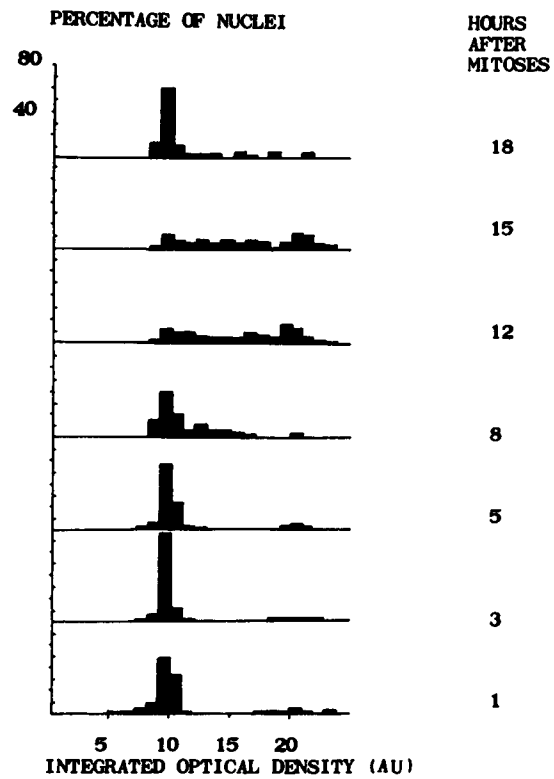


FIGURE 2 Integrated optical density histograms of Feulgen-stained nuclei from HeLa cells at various time intervals after synchronization by selective mitotic detachment (1, 3, 5, 8, 12, 15, and 18 h).

TABLE I

MEAN AND SD VALUES OF IOD AND SPECIFIC ACTIVITY OF HeLa S3 CELLS AFTER [$^3$H]THYMIDINE PULSE AT VARIOUS TIME INTERVALS AFTER SELECTIVE MITOTIC DETACHMENT (1)

| Time after mitosis | [$^3$H]thymidine Incorporation | IOD |
|---|---|---|
| *h* | *cpm* | $AU \times 10^3$ |
| 1 | 200 ± 50 | 11.6 ± 3.0 |
| 3 | 250 ± 40 | 10.0 ± 2.0 |
| 5 | 210 ± 50 | 9.9 ± 2.2 |
| 8 | 2,200 ± 380 | 10.4 ± 2.0 |
| 12 | 8,900 ± 1,800 | 13.4 ± 3.9 |
| 15 | 4,050 ± 2,080 | 14.8 ± 4.0 |
| 18 | 600 ± 400 | 10.2 ± 2.1 |

indicate a larger nuclear area (and perimeter) at 1 h than at both 3 and 5 h, even if DNA content (IOD) remains constant. Similar increases in area (and perimeter) occur during the transition of early S (8 h) to middle-late S (12 h), with a decrease down to the original mean value of middle G1 (61 $\mu m^2$ for area and 30 $\mu m$ for perimeter at 3 h) when the cells progress through G2 into the G1 phase of a new cell cycle (18 h). The same modulation of nuclear geometry appears evident from the variation of average optical density (Fig. 4) and form factor (Fig. 5), even within the same phase and at the transitions between phases. Specifically, a progressive marked shift toward lower

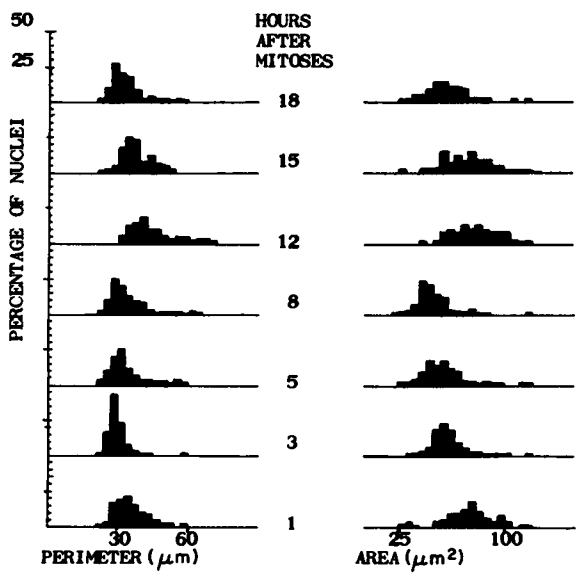


FIGURE 3. Area (right) and perimeter (left) histograms of Feulgen-stained nuclei from HeLa cells at various time intervals after synchronization by selective mitotic detachment (1, 3, 5, 8, 12, 15, and 18 h).

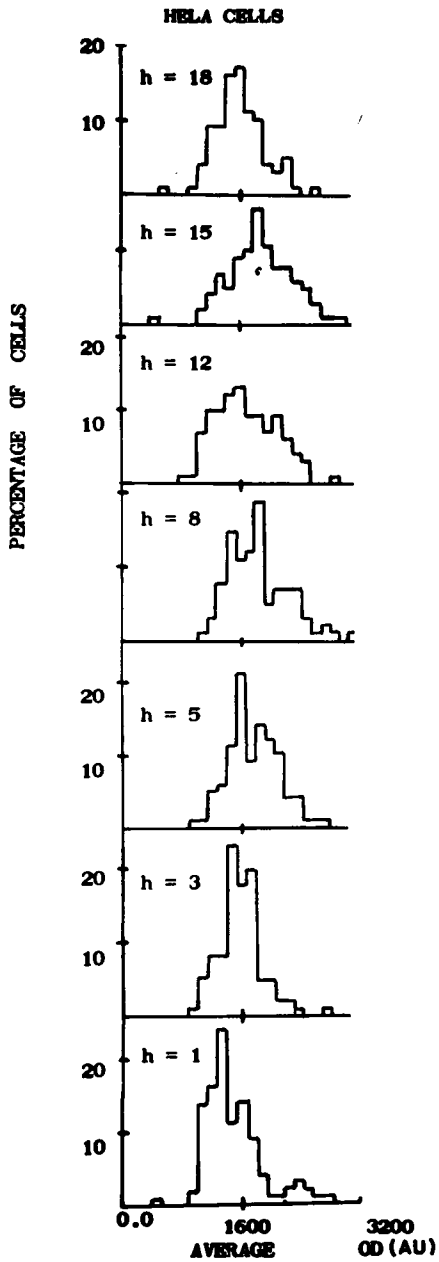


FIGURE 4

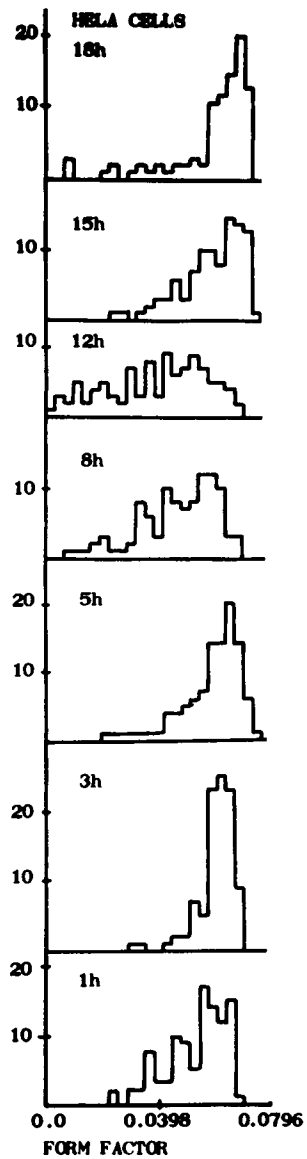


FIGURE 5

FIGURE 4 Average optical density histogram of Feulgen-stained nuclei from HeLa cells, at various times (h) after mitosis.

FIGURE 5 Form factor histograms of Feulgen-stained nuclei from HeLa cells, at various times (h) after mitosis.

values appears evident in the frequency distributions of both average optical density (i.e., increased chromatin dispersion) and form factor (i.e., increased chromatin convolution) when the cell goes from late G1 (5 h) to early S (8 h) and then to middle-late S (12 h). Both parameters increase significantly during the cell progression from early G1 (1 h) to middle (3 h) and late G1 (5 h) and at the transition between late S (12 h) and G2 (15 h). Interestingly enough, when the cells (after their first cycle after selective mitotic detachment) return to G1 phase (18 h), all the parameters, directly measured (Figs. 2 and 3) and derived (Figs. 4 and 5), return to the same mean values and frequency distributions of middle G1 (3 h).

*Threshold Dependence of Geometric Parameters*

Figs. 6, 7, 8, and 9 show area (Fig. 6), projection (Fig. 7), perimeter (Fig. 8), and MDP (Fig. 9) of Feulgen-stained HeLa S3 nuclei *in situ* vs. threshold from 0.04 OD, defining

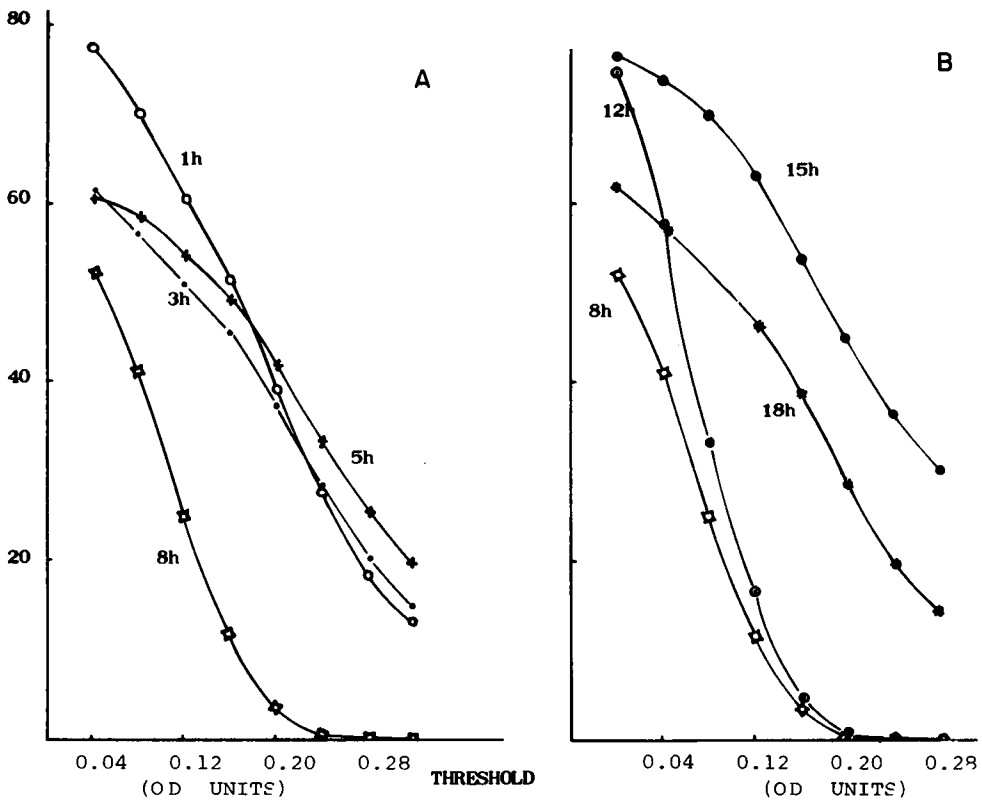


FIGURE 6 Mean values of the area ($\mu m^2$) of Feulgen-stained nuclei of S3 HeLa cells at seven different times after mitotic detachment (1, 3, 5, 8, 12, 15, and 18-h levels) versus threshold from 0.04 OD (defining the nuclear border of each image) to a maximum value of 0.32 OD with equal spacing of 0.04. The average points versus threshold are obtained on the same constant number of cells (about 100), including zero values at high threshold.

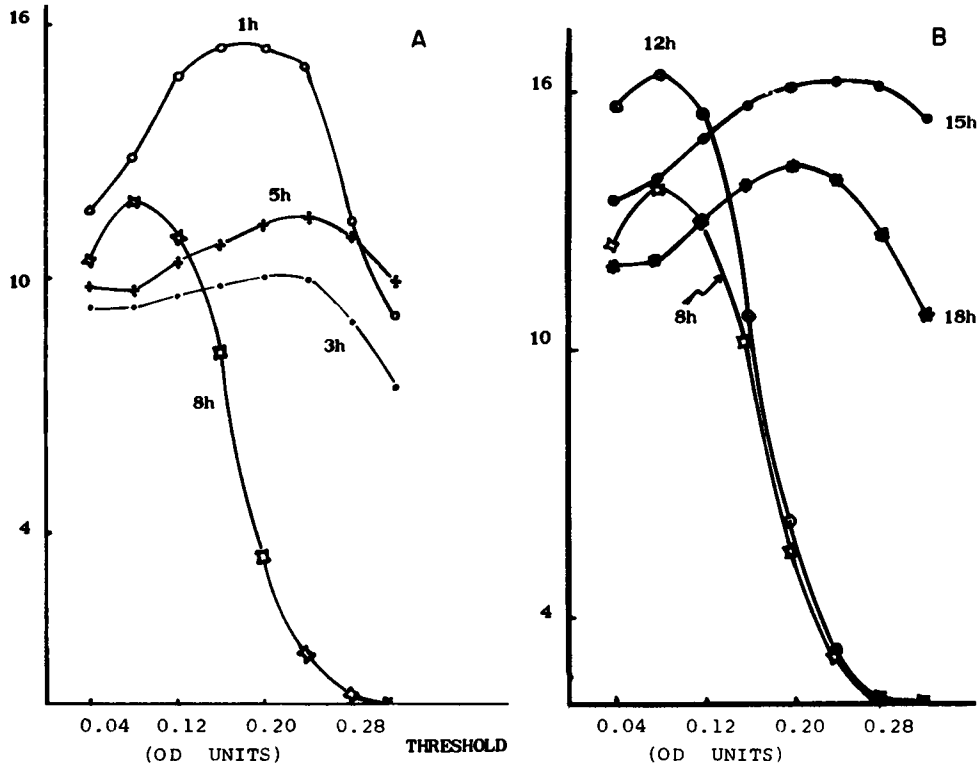


FIGURE 7 Projection mean values ($\mu$m) of Feulgen-stained nuclei of HeLa S3 cells at 1, 3, 5, 8, 12, 15, and 18 h after mitoses versus thresholds (0.04—0.32 OD). The projection is defined as the linear sum of all lagging edges projected against a vertical line.

the nuclear border of each cell image, to a maximum value of 0.32 OD, with equal spacing of 0.04 OD. Figs. 6–9 show the results obtained at 1, 3, 5, 8, 12, 15, and 18 h after mitotic detachment. At 8 and 12 h after mitoses the mean values of area, projection, and perimeter decrease drastically with increasing OD threshold, approaching zero already at a threshold equal to 0.24 OD. The corresponding values of MDP (Fig. 9) increase drastically with increasing OD threshold, going to infinity at the same threshold of 0.24 OD. Both phenomena are consistent with a high degree of chromatin dispersion during S phase. At 15 h the mean values of area (Fig. 6), projection (Fig. 7), and perimeter (Fig. 8) for OD thresholds larger than 0.12 are systematically higher than all other values obtained at the other times after mitoses, suggesting a high degree of chromatin condensation. At 18 h the mean values of area (Fig. 6) are practically identical at every threshold with those obtained at 3 h (Fig. 6); striking similarities of threshold dependence can be found between mean nuclear projections (Fig. 7) and perimeters (Fig. 8) at 3 h (middle G1 of first cycle) and 18 h (G1 of second cycle). It appears that a unique characterization of the nuclear morphometry of cells (independently of DNA content) can be achieved in middle G1 (at 3 and 18 h after

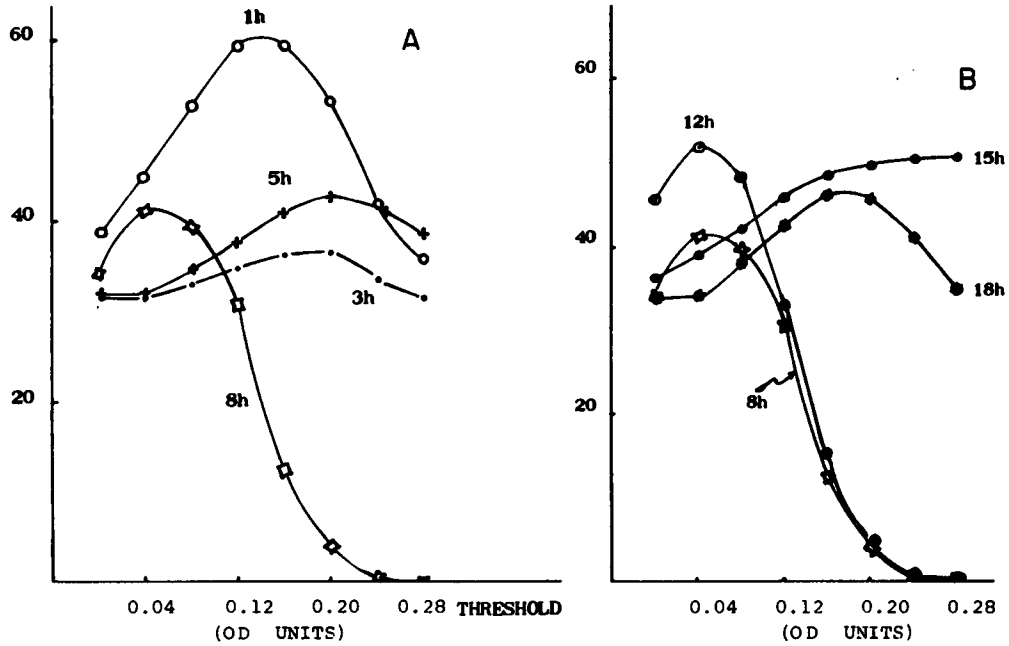


FIGURE 8 Perimeter mean values ($\mu$m) of Feulgen-stained nuclei from HeLa cells at 1, 3, 5, 8, 12, 15, and 18 h after mitoses, measured at eight different optical density levels (0.04 OD–0.32 OD)

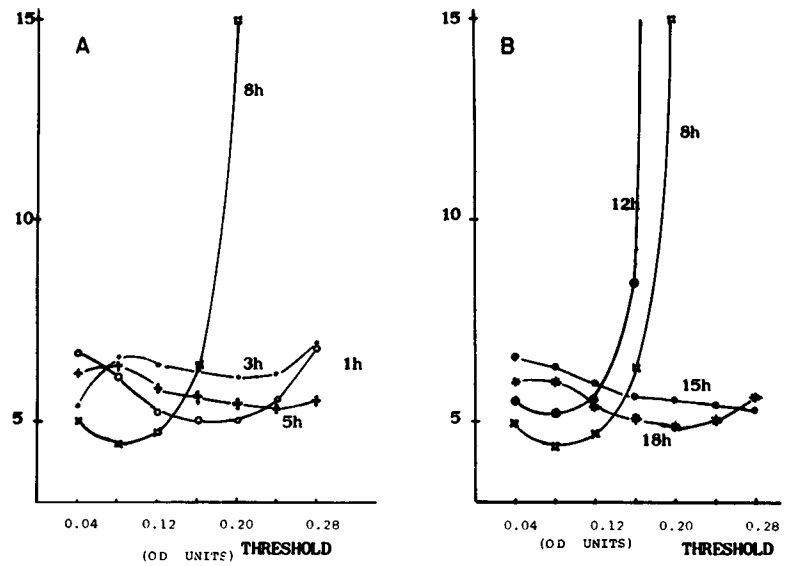


FIGURE 9 MDP for Feulgen-stained nuclei of HeLa S3 cells at 1, 3, 5, and 8 h (left) and 8, 12, 15, and 18 h (right) after selective mitotic detachment. MDP is defined as the ratio $(A_1 / Pr_i)$ of nuclear area $A_1$ at base threshold (0.04 OD) divided by the projection at threshold level $i$, where $i$ varies between 1 (0.04) and 8 (0.32).

mitoses), early S (8 h), late S (12 h), and G2 (15 h), which are consistent with previous findings at the level of isolated chromatin (1–7) and of the intact cell (15). Furthermore, objective identification of subphases and transitions between phases appears possible.

Consider the patterns of area (Fig. 6), projection (Fig. 7), perimeter (Fig. 8), and MDP (Fig. 9) at 5 h (late G1) and 8 h (early S) after mitoses. At the base threshold the mean values (15) of these parameters are either similar (projection and perimeter), or slightly different (area and MDP). However, the threshold-dependencies of these four parameters are strikingly different between late G1 and early S. Specifically, while the area, perimeter, and projection at 8 h decrease abruptly, reaching zero value at 0.24 OD, the area at 5 h has a finite mean value of 18 $\mu m^2$ even at the maximum threshold (0.32 OD); the perimeter (Fig. 3) and projection (Fig. 7) of the same 5-h population actually increase with increasing threshold and reach a final value, at the higher threshold of 0.32 OD, equal to (projection) or larger than (perimeter) the original one at the base threshold. At the same time, while the MDP of late G1 nuclei is practically independent of threshold levels, the MDP of early S nuclear images dramatically increases, going to infinity at a threshold of 0.24 OD. All phenomena are consistently compatible with chromatin dispersion during the G1-S transition, where only minor or no variation of DNA content occurs (Fig. 2) (Table I). Similarly, identification of discrete variations within the G1 phase (1, 3, and 5 h) in nuclear morphometry (area, perimeter, and projection), statistically indistinguishable at the base threshold (15) (Figs. 6–8), becomes possible by the analyses of their threshold dependencies. Specifically, the values obtained at 1 and 3 h and at 1 and 5 h are statistically different by a multivariate Student $t$ test at the 1% level, for lower and intermediate values of OD in projection (Fig. 7) and perimeter (Fig. 8); furthermore, the threshold dependence of area shows a much higher slope at 1 h than at 3 and 5 h. Finally, the patterns of area, projection, and perimeter of 3 and 5 h are statistically different at the 1% level for the last three highest values of threshold.

## DISCUSSION

Previous chemical and physicochemical studies (1–7) of chromatin isolated from bulk populations of synchronized cells have suggested that significant conformational changes take place during the cycle of mammalian cells. Specifically, in synchronized HeLa S3 cells, chromatin molar ellipticity at 276 nm (DNA conformation) and chromatin binding sites for ethidium bromide (1) increase abruptly between M and G1, remain constant during the entire G1, increase during the S phase up to 11 h (middle-S) and then decrease during G2 phase. Recent observations (15) of mean values of various geometric and densitometric parameters of Feulgen-stained nuclei from the same HeLa cells prove that substantial alterations of nuclear morphology during the cell cycle do exist even *in situ*, suggesting that conformational changes in chromatin are not artifacts resulting from alteration induced during the isolation procedure (8, 9). However, values of every single geometric parameter were distributed around their

mean values, with the distributions showing significant overlap between any two given times after detachment; the large standard deviations (15) (Table I) are consequences of the lack of homogeneity in any cell population, which show increasingly multi-modal distributions (see Fig. 2), with increasing time intervals after mitoses, as the cells become progressively desynchronized during their traverses in the cell cycle (1) (Fig. 2 and Table I). The occasional establishment of any significant differences among different cell cycle phases and their subphases has then been made possible only by a complex statistical analysis at a 2.5% confidence level (15). To identify objectively the nuclear geometry of each of the cell cycle phases and subphases, we further extended the analysis to (*a*) the frequency distributions of directly measured (Figs. 2–3) and derived (Figs. 4–5) parameters at the base threshold, and (*b*) the dependencies of their mean values upon thresholds (Figs. 6–9). The first analysis could allow us to identify, within any given multimodal distribution, subpopulations with specific geometric and densitometric properties: a two-dimensional scatter plot (not shown) consistently indicates that a decrease in average optical density is associated with a decrease in form factor, as shown previously for WI-38 cells stimulated to proliferate (10). The threshold dependence of nuclear geometry (Figs. 6–9) shows that a cell population that has a decrease in both form factor and average OD (8 and 12 h) also presents the following unique systematic features compatible with higher chromatin dispersion: (*a*) the area, perimeter, and projection of their nuclear images goes rapidly to zero at an intermediate threshold (0.24 OD); (*b*) the MDP increases, with threshold approaching infinity at an intermediate threshold (0.24 OD). The significance of these last findings is that, while geometric data at base threshold show substantial overlap and differences can be ascribed only by statistical analyses (15) or by peak localization of their multimodal frequency distributions (Figs. 2–4), the threshold dependence of each geometric parameter shows unique features (without any overlap) for each post-mitotic detachment time. This allows unique, model-independent assignment of the nuclear geometry of each cell cycle phase and its early, middle, and late subphases, even when measured DNA content (the most commonly utilized cell cycle descriptor to date) does not vary. A new redefinition of the cell cycle is then possible with the objective geometric and densitometric descriptors introduced in this paper. The following conclusions can be drawn:

(*a*) G1 phase can be objectively divided into three segments (or subphases): early G1 (1 h), middle G1 (3 h), and late G1 (5 h), by their characteristic threshold dependence of area (Fig. 6), perimeter (Fig. 8), and projection (Fig. 7). The increased optical density per unit area (Fig. 4), and increased form factor (Fig. 5) going from 1 to 5 h are compatible with both increased chromatin condensation and decreased convolution toward circular geometry. Within the G1 phase (1, 3, 5, and 18 h) the DNA content remains constant (10,000 AU), as indicated by the frequency distributions of IOD (Fig. 2). The frequency distributions of geometric parameters at base threshold and their mean values versus threshold are strikingly identical for nuclei at 18 h (G1 of the second cycle) and 3 h (middle G1 of first cycle) after mitosis.

(*b*) The transition between late G1 (5 h) and early S (8 h) phases, where most antimetabolites act and variations in DNA content are minimal (Table I), can be objectively characterized. In fact, the nuclear morphology changes abruptly in the direction of a decreased form factor (Fig. 5). Furthermore, the threshold dependence (Fig. 6–9) of the area, perimeter, projection, and MDP makes apparent this transition to a more disperse chromatin, compatible with a lower degree of DNA supercoiling (26). The directly measured parameters go to zero at the same threshold (0.24 OD) at which the derived MDP goes to infinity.

(*c*) The transition from early S (8 h) to middle-late S (12 h) is also now apparent by the further substantial decrease of both form factor (Fig. 5) and average OD (Fig. 4). The increase in chromatin dispersion is also made evident by the threshold dependence of nuclear MDP, perimeter, projection, and area. These changes of nuclear morphology during S phase are compatible with the conformational chromatin changes (1–5) and the increased metabolic activity of the cell (larger convolution is consistent with larger surface to volume ratio for the nuclei).

(*d*) The transition from late S (12 h) to G2 (15 h), where the frequency distributions of DNA content show only little variation toward larger values (Table I and Fig. 2), but where an increase of form factor (Fig. 5) appears evident. The decreased convolution toward circular geometry is accompanied by an increased chromatin condensation during this transition, as indicated by the threshold dependencies of the geometric parameters (Figs. 6–8), which show increasing values with increasing threshold for 15 h (G2), while they are already decreased to zero at threshold equal to 0.24 OD for 12 h (middle-late S).

(*e*) A distinction can be made between "G2" (15 h) and "G1" (18 and 3 h), also in terms of chromatin condensation (G2 has a larger average OD than G1; see Fig. 4) and by the threshold dependencies of projection (Fig. 7) and perimeter (Fig. 8), whose mean values progressively diverge with increasing threshold level until 0.32 OD, where little or no overlap exists between the frequency distributions of any parameter of these two cell populations. It is comforting to note that *all* parameters, after their abrupt and correlated variations during an entire cell cycle, do indeed return at their original middle G1 value (3 h) when they progress into the second cycle, specifically into a new G1 phase at 18 h (Fig. 2). Differences in the chromosome cycle, visualized by light microscopy only during mitosis, are then resolved also during interphase by the proper geometric and densitometric texture analysis conducted on Feulgen-stained HeLa cells. It must be stressed that only the combination of two or more parameters (form factor, MDP, average OD) derived from three or more direct measurements (IOD, area, perimeter, and projection), allows objective determination of cell cycle phases and their segments on the basis of chromatin geometry, to an extent not possible by simply measuring a single parameter such as DNA content. A single, directly measured parameter (including the geometric ones) has never been observed by us to be other than distributed, with considerable overlap between various phases, and is only interpretable by a

model in the absence of any other observable measurement. In conclusion, by the simultaneous evaluation of derived parameters at base threshold and directly measured parameters versus threshold of Feulgen-stained cells, a cell in a given subphase (i.e., late G1) can be objectively distinguished from a cell in a different subphase (i.e. middle G1) to an extent up to now impossible to any human observer. These measurements could become useful to cell biologists and cytopathologists (25), as already shown in the objective characterization of the nonproliferating G0 compartment in the G0–G1 transition of WI-38 cells (10, 15). Automated image analysis therefore represents a quantum jump in quality (new and more accurate observables) and quantity (speed of data acquisition and reduction, and adequate sample sizes) of cell characterization with respect to traditional autoradiography (lengthy, limited, and sometimes misleading [4]), and even laser flow microfluorimetry (by virtue of the problems inherent in obtaining homogeneous cell suspensions from tissues in intact animals [25]).

This work was supported by National Cancer Institute Grants CA20034 and CA18258.

*Received for publication 13 December 1976 and in revised form 5 May 1977.*

## REFERENCES

1. NICOLINI, C., K. AJIRO, T. W. BORUN, and R. BASERGA. 1975. Chromatin change during the HeLa cell cycle, *J. Biol. Chem.* **250**:3381.
2. NICOLINI, C. 1975. The discrete phases of the cell cycle: autoradiographic, physical and chemical evidences. *J. Natl. Cancer Inst.* **55**:821.
3. BASERGA, R., and C. NICOLINI. 1975. Chromatin structure and function in proliferating cells. *Biochim. Biophys. Acta.* **458**:109.
4. PEDERSON, T., and E. ROBBINS. 1972. Chromatin structure and the cell division cycle. Actinomycin binding in synchronized HeLa cells. *J. Cell Biol.* **55**:322.
5. PEDERSON, T. 1972. Chromatin structure and the cell cycle. *Proc. Natl. Acad. Sci. U.S.A.* **69**:2224.
6. MARKS, D., W. K. PAIK, and T. BORUN. 1974. Relationship of histone phosphorylation with deoxyribonucleic acid replication and mitosis during HeLa S3 cell cycle. *J. Biol. Chem.* **248**:5660.
7. BELLHORNE, R., J. BORDWELL, and L. SELLERS. 1972. Histone phosphorylation and DNA synthesis are linked in synchronous culture of HTC cells. *Biochim. Biophys. Res. Commun.* **46**:1326.
8. NOLL, M., T. THOMAS, and R. KOERNBERG. 1975. Preparation of native chromatin and damage caused by shearing. *Science, (Wash. D.C.).* **187**:1203.
9. NICOLINI, C., R. BASERGA, and F. KENDALL. 1976. DNA structure in sheared and unsheared chromatin. *Science (Wash. D.C.).* **192**:796.
10. KENDALL, F., S. WU, W. GIARRETTI, and C. NICOLINI. 1977. Multiparameter geometric and densitometric analysis of the G0–G1 transition of WI-38 cells, *J. Histochem. Cytochem.* In press.
11. TER MEULEN, V., P. H. BARTELS, G. F. BAR, M. BIBBO, N. CREMER, E. H. LENNETTE, and G. G. WIED. 1972. Computer-assisted analysis of a carrier culture infected with Moloney leukemia virus. *Acta Cytol.* **16**:454.
12. BARTELS, P. H., G. B. OLSON, J. M. LAYTON, R. E. ANDERSON, and G. L. WIED. 1975. Computer discrimination of T and B lymphocytes. *Acta Cytol.* **19**:53.
13. NICOLINI, C., W. GIARETTI, and F. KENDALL. 1975. G0–G1 transition in WI-38 cells. II. Geometric and densitometric analysis. *Exp. Cell. Res.* **106**:119.
14. SAWICKI, W., J. ROWINSKI, and R. SWENSON. 1974. Change of chromatin morphology during the cell cycle detected by means of automated image analysis. *J. Cell. Physiol.* **84**:423.
15. KENDALL, F., R. SWENSON, J. ROWINSKI, T. BORUN, and C. NICOLINI. 1977. Nuclear morphometry during cell cycle. *Science (Wash. D.C.).* **196**:1106.

16. FISHER, C. 1971. The new quantimet 720. *Microscope.* **19**:848.
17. FISHER, C., and C. P. BOND. 1972. The Quantimet, 720D for densitometry in life science. *Microscope.* **20**:203.
18. PETERSON, D. F., R. A. TOBEY, and E. L. ANDERSON. 1969. Synchronized dividing mammalian cells. *Fed. Proc.* **28**:1771.
19. TERASIMA, T., and I. J. TOLMACH. 1963. Growth and nucleic acid synthesis in synchronized dividing populations of HeLa cells. *Exp. Cell Res.* **30**:344.
20. ROBBINS, E., and P. I. MARCUS. 1964. Mitotic synchronization of mammalian cells: a simple method for obtaining large populations. *Science (Wash. D.C.).* **144**:1152.
21. STEIN, G., and T. BORUN. 1972. Synthesis of acidic chromosomal protein during the cell cycle of HeLa S3 I. Accelerated accumulation of acidic residual nuclear proteins before the initiation of DNA replication. *J. Cell Biol.* **52**:292.
22. DE COSSE, I. J., and N. AIELLO. 1966. Feulgen hydrolisis: effect of acid and temperature" *J. Histochem. Cytochem.* **14**:501.
23. DIXON, W. J., and F. J. MASSEY, JR. 1969. Introduction to Statistical Analysis. McGraw-Hill Book Company, New York. 308.
24. KENDALL, F. M., G. LOFFREDO, and C. NICOLINI. 1975. Computer programs for shape and densitometric analysis. Internal Report 7/75, Biophysics Div., Temple University Health Science Center, Philadelphia.
25. NICOLINI, C. 1976. The principles and methods of cell synchronization and cancer chemotherapy. *Biochim. Biophys. Acta.* **458**:243.
26. NICOLINI, C., and F. KENDALL. 1977. Differential light scattering in native chromatin. Corrections and inferences combining melting and dye binding studies. A two-order superhelical model, *Physiol. Chem. Phys.* In press.